

4

AD-A210 264

Bias and Oxide Thickness Dependence of Trapped Charge Buildup in MOS Devices

Prepared by

R. J. KRANTZ and T. C. ZIETLOW
Electronics Research Laboratory
The Aerospace Corporation
El Segundo, CA 90245

DTIC
ELECTE
JUL 19 1989
S
D
D

31 January 1989

Prepared for

SPACE DIVISION
AIR FORCE SYSTEMS COMMAND
Los Angeles Air Force Base
P.O. Box 92960
Los Angeles, CA 90009-2960

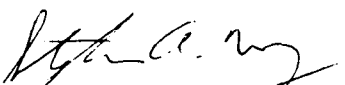
APPROVED FOR PUBLIC RELEASE;
DISTRIBUTION UNLIMITED

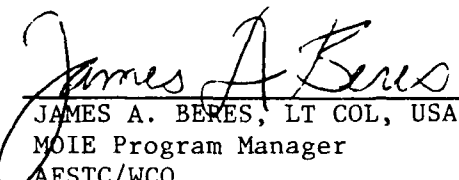
This report was submitted by The Aerospace Corporation, El Segundo, CA 90245, under Contract No. F04701-88-C-0089 with the Space Division, P.O. Box 92960, Los Angeles, CA 90009. It was reviewed and approved for The Aerospace Corporation by M. J. Daugherty, Director, Electronics Research Laboratory.

Lt. Steve Way was the project officer for the Mission-Oriented Investigation and Experimentation (MOIE) Program.

This report has been reviewed by the Public Affairs Office (PAS) and is releasable to the National Technical Information Service (NTIS). At NTIS, it will be available to the general public, including foreign nationals.

This technical report has been reviewed and is approved for publication. Publication of this report does not constitute Air Force approval of the report's findings or conclusions. It is published only for the exchange and stimulation of ideas.


STEPHEN A. WAY, LT, USAF
MOIE Project Monitor
AFSTC/WCO


JAMES A. BERES, LT COL, USAF
MOIE Program Manager
AFSTC/WCO

UNCLASSIFIED

SECURITY CLASSIFICATION OF THIS PAGE

REPORT DOCUMENTATION PAGE				
1a. REPORT SECURITY CLASSIFICATION Unclassified		1b. RESTRICTIVE MARKINGS		
2a. SECURITY CLASSIFICATION AUTHORITY		3. DISTRIBUTION/AVAILABILITY OF REPORT Approved for public release; distribution unlimited		
2b. DECLASSIFICATION/DOWNGRADING SCHEDULE				
4. PERFORMING ORGANIZATION REPORT NUMBER(S) TR-0089(4925-07)-1		5. MONITORING ORGANIZATION REPORT NUMBER(S) SD-TR-89-42		
6a. NAME OF PERFORMING ORGANIZATION The Aerospace Corporation Laboratory Operations	6b. OFFICE SYMBOL (If applicable)	7a. NAME OF MONITORING ORGANIZATION Space Division		
6c. ADDRESS (City, State, and ZIP Code) El Segundo, CA 90245		7b. ADDRESS (City, State, and ZIP Code) Los Angeles Air Force Base Los Angeles, CA 90009-2960		
8a. NAME OF FUNDING/SPONSORING ORGANIZATION	8b. OFFICE SYMBOL (If applicable)	9. PROCUREMENT INSTRUMENT IDENTIFICATION NUMBER		
8c. ADDRESS (City, State, and ZIP Code)		10. SOURCE OF FUNDING NUMBERS		
		PROGRAM ELEMENT NO.	PROJECT NO.	TASK NO.
		WORK UNIT ACCESSION NO.		
11. TITLE (Include Security Classification) Bias and Oxide Thickness Dependence of Trapped Charge Buildup in MOS Devices				
12. PERSONAL AUTHOR(S) Krantz, R. J., and Zietlow, T. C.				
13a. TYPE OF REPORT	13b. TIME COVERED FROM _____ TO _____	14. DATE OF REPORT (Year, Month, Day) 1989 January 31	15. PAGE COUNT 24	
16. SUPPLEMENTARY NOTATION				
17. COSATI CODES			18. SUBJECT TERMS (Continue on reverse if necessary and identify by block number)	
FIELD	GROUP	SUB-GROUP		
			Oxides, Charge Buildup, Sweep-out, Trapping, Tunneling, Recombination	
19. ABSTRACT (Continue on reverse if necessary and identify by block number) A rate equation for charge buildup, which includes sweep-out, hole/electron trapping, tunneling, recombination, and the effects of internal fields, is generalized to apply to negative gate biases and include electron injection from the silicon and aluminum gate interfaces. The dependence of the midgap voltage shift on oxide thickness is explicitly examined. The theoretical results are verified by comparison with experimental results obtained on p-type silicon test capacitors of different oxide thicknesses under varying positive and negative gate biases.				
20. DISTRIBUTION/AVAILABILITY OF ABSTRACT <input checked="" type="checkbox"/> UNCLASSIFIED/UNLIMITED <input type="checkbox"/> SAME AS RPT. <input type="checkbox"/> DTIC USERS			21. ABSTRACT SECURITY CLASSIFICATION Unclassified	
22a. NAME OF RESPONSIBLE INDIVIDUAL			22b. TELEPHONE (Include Area Code)	22c. OFFICE SYMBOL

ACKNOWLEDGMENTS

The authors would like to thank L. W. Aukerman for his assistance.



Accession For	
NTIS GRA&I	J
DTIC TAB	<input type="checkbox"/>
Unannounced	<input type="checkbox"/>
Justification	
By	
Distribution /	
Availability Codes	
A-1	

CONTENTS

I.	INTRODUCTION	5
II.	THEORY	7
III.	EXPERIMENTAL COMPARISON	19
IV.	SUMMARY	25
	REFERENCES	27

FIGURES

1.	Theoretical Results for the Magnitude of the Initial Midgap Voltage Shift per Dose versus Field Across a 750 and 500 Å Oxide Using Parameters Cited in the Literature	12
2.	Theoretical Results for the Charge Distribution versus Thickness in a Typical Oxide for Positive and Negative Applied Fields of Magnitude 5 MV/cm	14
3.	Theoretical Results for the Maximum Midgap Shift versus Applied Field for a 750 Å Oxide in Various Limits of the Theory	16
4.	Typical Data for the Magnitude of the Initial Slope versus Applied Field	20
5.	Composite of the Initial Slope versus Applied Field Data for the Oxides Studied	21
6.	Composite of the Maximum Midgap Voltage Shift Data for the Oxides Studied	23

TABLES

1.	Parameters Used to Generate Theoretical Results	22
----	-------------------------------------------------------	----

I. INTRODUCTION

Recently [1], a description of trapped charge buildup in MOS devices under positive gate bias was developed based on physical mechanisms that included carrier sweepout [2-7, 13-15, and 17], radiation-induced electron-hole pair generation [2-17], recombination [2-7, 13-15, and 17], field-dependent hole/electron trapping [2-7, 10, 13-17], tunneling at large doses [3, 5, and 6] and the effects of internal fields. Experimentally accessible factors of import to the description of charge trapping in oxides are: the total absorbed dose, applied field, oxide thickness, and temperature [1-7]. Because the threshold voltage shift depends on the first moment of the charge distribution [18], the spatial dependence of this distribution is important.

In the following section, we extend the description for the oxide trapped charge distribution in a low dose rate environment to include: (1) negative gate biases, (2) tunneling at low doses, (3) low applied fields, and (4) the effect of electron injection at the interfaces. In the subsequent section, experimental results for the initial midgap shift per dose and the maximum midgap voltage as a function of field are compared to the theoretical results.

II. THEORY

We begin by considering the continuity equation for trapped holes:

$$dN_p/dt = \sigma_{dp}j_p(N_{Tp} - N_p) - \sigma_{cn}j_nN_p \quad (1)$$

where

- N_p = trapped hole concentration
- σ_{dp} = the dipole-induced hole capture cross section (neutral hole traps)
- σ_{cn} = coulombic electron capture cross section
- j_p = radiation-induced hole flux
- j_n = radiation-induced electron flux
- N_{Tp} = concentration of neutral oxide hole traps.

The first term on the right-hand side of Eq. (1) describes hole trapping by neutral (induced-dipole) traps. The trapping rate is proportional to the induced dipole capture cross section σ_{dp} ; the hole current j_p ; and the number of unfilled neutral traps ($N_{Tp} - N_p$). The second term describes the rate at which filled hole traps capture electrons and become neutral. The filled hole trap is a coulombic center. The coulombic trapping rate for electrons is proportional to the coulombic capture cross section σ_{cn} ; the electron current j_n ; and the concentration of filled hole traps N_p .

Similarly, the continuity equation for trapped electrons is:

$$dN_n/dt = \sigma_{dn}j_n(N_{Tn} - N_n) - \sigma_{cp}j_pN_n \quad (2)$$

where

- N_n = trapped electron concentration
- σ_{dn} = the dipole-induced electron capture cross section (neutral electron traps)
- σ_{cp} = coulombic hole capture cross section
- N_{Tn} = concentration of neutral oxide electron traps.

The first term on the right-hand side of Eq. (2) describes the neutral (induced-dipole) trapping kinetics for electrons. The second term describes hole trapping by filled electron traps analogous to electron trapping by filled hole traps described above.

As has been discussed elsewhere [1], the radiation-induced hole and electron flux may be derived from the conduction band electron and valence band hole continuity equations. The conduction band electron continuity equation is:

$$dn/dt = dj_n/dx + n_o\dot{D}\varphi - j_n[\sigma_{cn}N_p + \sigma_{dn}(N_{Tn} - N_n)] \quad (3)$$

where

- n = conduction band electron concentration
- n_o = electron-hole pairs generated per dose
- \dot{D} = dose rate
- φ = electron-hole escape probability.

Similarly, the valence band hole continuity equation is:

$$dp/dt = -dj_p/dx + n_o\dot{D}\varphi - j_p[\sigma_{cp}N_n + \sigma_{dp}(N_{Tp} - N_p)] \quad (4)$$

where

- p = valence band hole concentration.

In a low dose rate, high total dose environment, these equations may be solved in steady state [1]. Also, it has been shown that under these conditions the radiation-induced carrier generation terms dominate the capture terms [1]. Under positive gate bias, Eqs. (3) and (4) may be solved to yield:

$$j_{n+} = j_{n0} + n_o\dot{D}\varphi(t_{ox} - x) \quad (5a)$$

and

$$j_{p+} = j_{p0} + n_o\dot{D}\varphi x \quad (5b)$$

where t_{ox} is the oxide thickness and j_{n0} and j_{p0} are the electron and hole injection currents, respectively. The origin of the coordinates is at the gate electrode.

Under negative gate bias the electron and hole fluxes are given by:

$$j_{n-} = -j_{n0} - n_o\dot{D}\varphi x \quad (6a)$$

and

$$j_{p-} = -j_{p0} - n_o\dot{D}\varphi(t_{ox} - x). \quad (6b)$$

Substituting for the electron and hole fluxes and effecting the integrations in Eqs. (1) and (2) yield the following form for the trapped charge distributions:

$$N_{i,s} = N_T f_{i,s}(x) [1 - \exp(-t/T_{i,s}(x))] \quad (7)$$

where the subscript i denotes either electrons, n , or holes, p , and the subscript s denotes the sign of the gate bias. The factor $f_{i,s}(x)$ has the following form:

$$f_{i,s} = \sigma_d \psi_{i,s} T_{i,s}(x) \quad (8)$$

and

$$T_{i,s} = j_{i,s}(\sigma_{di} - \sigma_{ci}) + \sigma_{ci} J_{i,s}/q \quad (9)$$

where

$$J_{i,s} = s(j_{i0} + qn_o D \phi_{ox}) \quad (10)$$

(the total current density;
note that s is just the sign
of the field in the oxide)

and i^* denotes that the capture cross section used is for the other charge species (i.e., if i refers to holes, i^* refers to electrons).

The net charge density in the oxide is proportional to the difference between the trapped hole distribution and the trapped electron distribution:

$$Q_{net,s} = q(N_{p,s} - N_{n,s}). \quad (11)$$

Substitution of Eqs. (7) - (10) into Eq. (11) yields a rather cumbersome result for the net charge density versus dose. The experimental quantities of import are the initial midgap voltage shift per dose and the maximum midgap voltage shift. These quantities depend on the extremes of Eq. (11). Therefore, we will proceed to a discussion of these extremes and the associated experimental quantities.

At early times, expansion of the net charge yields:

$$Q_{0,s} = qN_{Tp}(\sigma_{dp}j_{p,s} - f_T \sigma_{dn}j_{n,s})t \quad (12a)$$

where

$$f_T = N_{Tn}/N_{Tp} \quad (12b)$$

and t is the time. In order to calculate the initial midgap voltage shift per dose, the first moment of the early time charge distribution, Eq. (12a), must be calculated.

First, we assume that the holes may tunnel from the oxide into the semiconductor at the oxide/semiconductor interface and may also tunnel from the oxide into the metal at the oxide/gate interface. The importance of this mechanism has been shown previously [1]. We also assume that electrons may tunnel from the oxide into the semiconductor and the gate contact.

Under these conditions the low dose, midgap voltage shift is given by:

$$V_s = -s(q/\epsilon)N_{Tp}\sigma_d \left[\int_{\Delta x_{p,s}^{gate}}^{t_{ox} - \Delta x_{p,s}^{si}} x j_{p,s} dx - f_T \int_{\Delta x_{n,s}^{gate}}^{t_{ox} - \Delta x_{n,s}^{si}} x j_{n,s} dx \right] \quad (13)$$

where we have assumed that the dipole-induced (neutral) trap cross sections for holes and electrons are identical. The tunneling distances in the limits of the integrals above are, in general, different for holes and electrons at each interface for both positive and negative applied fields in the oxide. We have calculated the appropriate tunneling distances in the WKB approximation assuming the depth of the hole traps is 3 eV relative to the valence band and the depth of the neutral electron traps is 4 eV below the conduction band [1,9]. The electron tunneling mass at the silicon interface is assumed to be .94 free electron masses, and the tunneling mass at the aluminum contact is assumed to be .42 free electron masses [19]. Evaluation of Eq. (13) for both positive and negative applied fields yields the following for the initial slopes:

$$V_+/D = -(q/3\epsilon)N_{Tp}\sigma_d n_o \phi t_{ox}^3 G_+(\Delta x', f_T) \quad (14a)$$

and

$$V_-/D = -(q/3\epsilon)N_{Tp}\sigma_d n_o \phi t_{ox}^3 G_-(\Delta x', f_T) \quad (14b)$$

where

t_{ox} = the oxide thickness

$\Delta x'$ = the appropriate hole tunneling distances divided by t_{ox} .

The factors G_+ and G_- are given by:

$$\begin{aligned} G_+ = & [(1 - \Delta x'_{p+} S_i)^3 - (\Delta x'_{p+} gate)^3 + (j_{p0}/2n_o \phi \dot{D} t_{ox}) \\ & ((1 - \Delta x'_{p+} S_i)^2 - (\Delta x'_{p+} gate)^2)] \\ & - [f_T/2)(3/2 + j_{n0}/2n_o \phi \dot{D} t_{ox}) \\ & ((1 - \Delta x'_{n+} S_i)^2 - (\Delta x'_{n+} gate)^2) \\ & - (1 - \Delta x'_{n+} S_i)^3 + (\Delta x'_{n+} gate)^3] \end{aligned} \quad (15a)$$

$$\begin{aligned} G_- = & [(\Delta x'_{p-} gate)^3 - (1 - \Delta x'_{p-} S_i)^3 + (3/2 + \\ & j_{p0}/n_o \phi \dot{D} t_{ox})((1 - \Delta x'_{p-} S_i)^2 - (\Delta x'_{p-} gate)^2)] \\ & - [f_T((1 - \Delta x'_{n-} S_i)^3 - (\Delta x'_{n-} gate)^3 + \\ & j_{n0}/2n_o \phi \dot{D} t_{ox})((1 - \Delta x'_{n-} S_i)^2 - \\ & (\Delta x'_{n-} gate)^2)]. \end{aligned} \quad (15b)$$

The ratio of the negative to the positive applied field initial slopes is given by the ratio of G_- to G_+ . For thick oxides, such that all the $\Delta x'$ are much less than one, the initial slope ratio reduces to:

$$G_-/G_+ = (1/2 - f_T)/(1 - f_T/2) \quad (16)$$

In this limit, as long as the concentration of neutral electron traps is less than half that of the neutral hole traps ($f_T < 1/2$), the initial slopes for both negative and positive applied fields are negative, with the magnitude of the initial slope for positive fields being larger. If the neutral electron trap concentration is much smaller than the neutral hole trap concentration, the magnitude of the

positive field initial slope is twice the magnitude of the negative field initial slope. For neutral electron trap concentrations near, but smaller than, the neutral hole trap concentrations, the magnitude of the negative applied field initial slopes will be substantially less than the magnitude of the positive applied field initial slopes.

In Figure 1 we show the initial slope versus field across the oxide for typical values, cited in the literature [8], for the parameters listed. The zero field dipole and coulombic capture cross sections may be calculated [1] to be $\sim 8 \times 10^{-15} \text{ cm}^2$ and $\sim 2 \times 10^{-13} \text{ cm}^2$, respectively. No hole injection is assumed, and electron injection occurs at the gate contact only. Under these conditions the positive field initial slopes exceed the negative field results, although for the smaller thickness this difference is considerably smaller. As has been described elsewhere [1], the low field behavior is dominated by the increase in the yield with field. At high fields the field dependence is dominated by the decrease in the capture cross sections with field.

At the other extreme, long times, Eq. (11) with the help of Eq. (7) yields:

$$Q_{max,s} = qN_{Tp}\sigma_d(j_{p,s}T_{p,s} - f_T j_{n,s}T_{n,s}). \quad (17)$$

Using the assumptions cited above, the maximum midgap voltage shift is:

$$V_{max,s} = -qN_{Tp}\sigma_d \left(\int_{\Delta x_{p,s}^{gate}}^{t_{ox} - \Delta x_{p,s}^{Si}} x j_{p,s} T_{p,s} dx - f_T \int_{\Delta x_{n,s}^{gate}}^{t_{ox} - \Delta x_{n,s}^{Si}} x j_{n,s} T_{n,s} dx \right) \quad (18)$$

Evaluation of Eq. (18) using Eqs. (5), (6), and (9) yields:

$$V_{max,s} = -(q/\epsilon)N_{eff,s}t_{ox}^2 \quad (19a)$$

where

$$N_{eff+} = N_{Tp}\sigma_d' \left[\int_{\Delta x_{p+}^{gate}}^{1 - \Delta x_{p+}^{Si}} ((x'^2/(x' + \sigma_c'))dx' - f_T \int_{\Delta x_{n+}^{gate}}^{1 - \Delta x_{n+}^{Si}} (x'(1 - x')/(1 - x' + \sigma_c'))dx' \right]$$

and

$$N_{eff-} = N_{Tp}\sigma_d' \left[\int_{\Delta x_{p-}^{gate}}^{1 - \Delta x_{p-}^{Si}} (x'(1 - x')/(1 - x' + \sigma_c'))dx' - f_T \int_{\Delta x_{n-}^{gate}}^{1 - \Delta x_{n-}^{Si}} ((x'^2/(x' + \sigma_c'))dx' \right] \quad (19c)$$

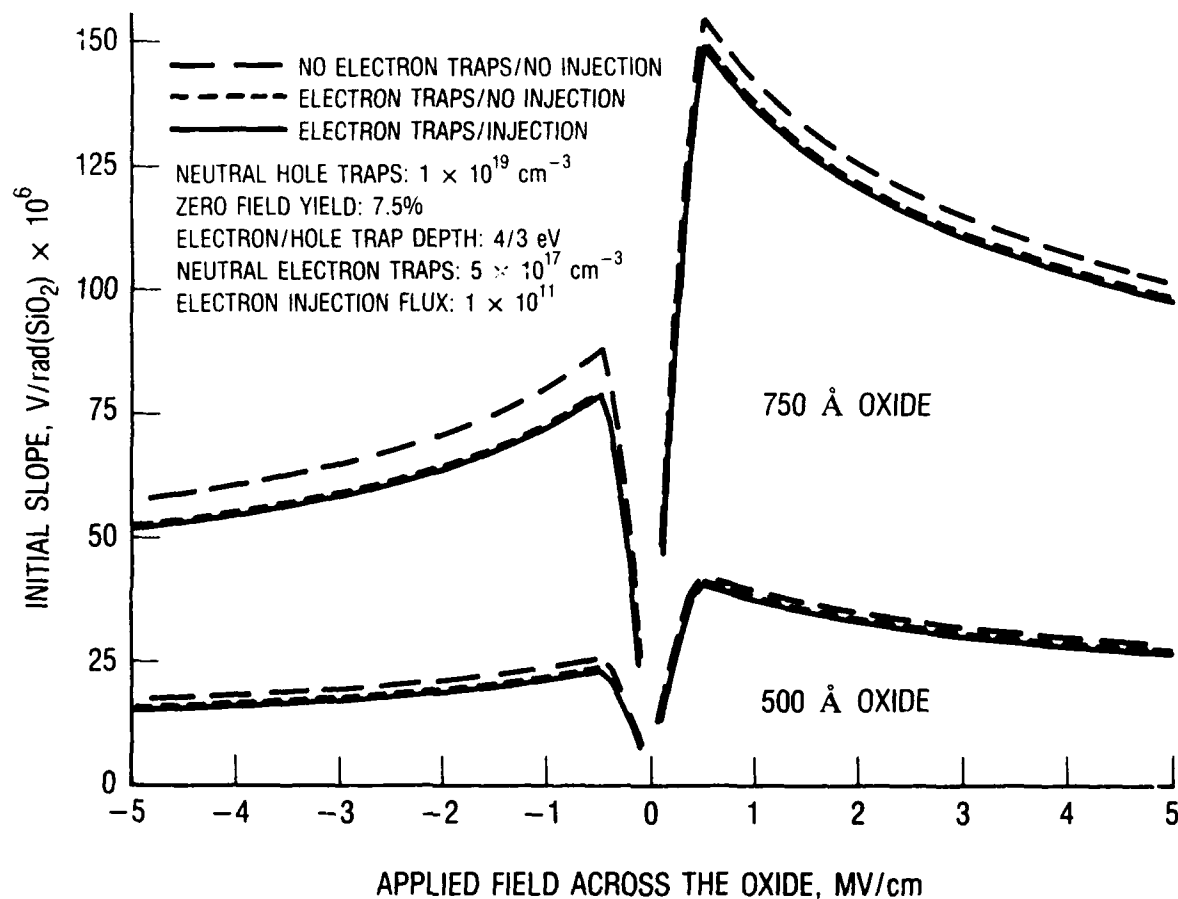


Fig 1. Theoretical Results for the Magnitude of the Initial Midgap Voltage Shift per Dose versus Field Across a 750 and 500 Å Oxide Using Parameters Cited in the Literature.

where it has also been assumed that the hole and electron coulombic capture cross sections are equal and

$$\sigma_d' = \sigma_d / (\sigma_d - \sigma_c) \quad (20a)$$

$$\sigma_c' = \sigma_c / (\sigma_d - \sigma_c). \quad (20b)$$

In the limit that $\Delta x'$ is zero and there are no neutral electron traps, $f_T = 0$, N_{eff+} reduces to a form previously published in the literature [1]. The ratio of N_{eff+} to N_{eff-} gives the ratio of the positive to negative applied field maximum midgap shift. In the limit of small $\Delta x'$ and no neutral electron traps, this ratio approaches a value of 6.8 for capture cross section ratios, σ_r , of 0.01, which is typical at low applied fields.

Shown in Figure 2 is the fraction (compared to the number of neutral hole traps, N_{Tp}) of trapped holes, electrons, and the net charge distribution for applied fields of +5 MV/cm and -5 MV/cm at saturation. Electron injection occurs at the gate contact only. For the positive field case, the trapped hole and electron distributions are zero within their respective tunneling distances of each interface. Note that at the gate interface ($x=0$) the hole and electron tunneling distances are approximately equal, while at the opposite interface these are different by about a factor of 2. As expected, the hole distribution is peaked near the silicon interface for positive field. The electron distribution is peaked near the gate interface for positive field. The significantly smaller peak value of the electron distribution is due to two factors. First, the concentration of electron traps is assumed to be significantly less than the concentration of hole traps (in this case N_{Tp} is $7.5 \times 10^{18} \text{ cm}^{-3}$, whereas N_{Tn} is $6 \times 10^{17} \text{ cm}^{-3}$) and the electron trap capture cross section is smaller ($\sim 10^{-14}$ compared to $\sim 10^{-12} \text{ cm}^2$). These values are consistent with those cited in the literature [8,9].

For negative fields the hole distribution is peaked near the gate and the electron distribution is peaked near the silicon interface. Because we have assumed that electron injection occurs at the gate only, this phenomenon only occurs for negative applied field. Because carrier injection, in this case electrons, provides a larger source of electrons for capture by neutral electron traps and by filled hole traps, the electron distribution for negative field is larger than for positive field (where no electron injection was assumed) and the hole distribution is smaller.

In these calculations the field dependence of the capture cross sections, discussed previously [1,7], has been assumed. Also, the fields, both positive and negative, have been corrected to account for the internal fields caused by the resulting radiation-induced charge densities. It can be shown by using techniques cited in the literature [20] that the field in the oxide may be calculated in the following way:

$$E(x) = (V_1 - V_2)/(x_2 - x_1) + (1/\epsilon(x_2 - x_1)) \left[\int_{x_1}^x (x' - x_1) \rho(x') dx' + \int_x^{x_2} (x' - x_2) \rho(x') dx' \right] \quad (21)$$

where

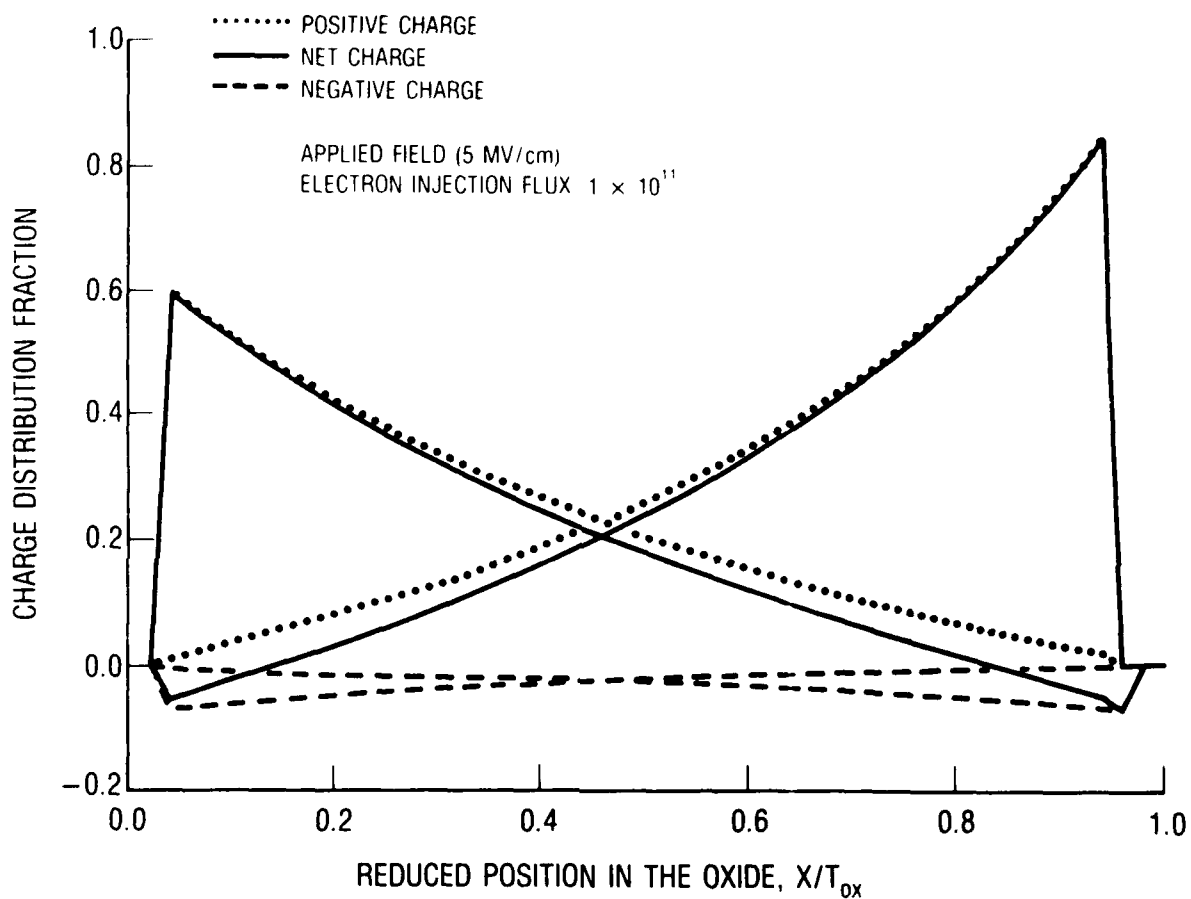


Fig 2. Theoretical Results for the Charge Distribution versus Thickness in a Typical Oxide for Positive and Negative Applied Fields of Magnitude 5 MV/cm. Electron injection has been included for the negative field results.

V_1 = the potential at x_1

V_2 = the potential at x_2

and ρ is the appropriate charge density. We may calculate the average field in the oxide by integrating the field in the oxide, Eq. (21), over the region in which charges reside in the oxide, obtaining:

$$E_s = [1/(t_{ox} - \Delta x_s)] \int_{\Delta x_{n,s}^{gate}}^{t_{ox} - \Delta x_{n,s}^{Si}} E(x) dx \quad (22)$$

where

Δx_s = the thickness over which no charge resides in the oxide due to tunneling. (Because the electron tunneling thicknesses are smaller than the hole tunneling thicknesses, this is just equal to $\Delta x_{n,s}^{Si} + \Delta x_{n,s}^{gate}$). Recall that s is the index which refers to the sign of the applied field.

After some manipulation the average field may be written as:

$$E_s = E_a + \Delta x'_{n,s} \Delta V_{max,s} / [t_{ox}(1 - \Delta x'_{n,s})] + \Delta x'_{n,s}^{gate} t_{ox} / [\epsilon(1 - \Delta x'_{n,s})] \int_{\Delta x'_{n,s}^{gate}}^{1 - \Delta x'_{n,s}^{Si}} Q_{max,s} dx' \quad (23)$$

In the following we have used Eq. (23) to describe the field in the oxide and evaluated all the field-dependent quantities using E_s rather than the applied field, E_a . Because the maximum threshold voltage shift $\Delta V_{max,s}$ and the charge distribution $Q_{max,s}$ depend on the field E_s , Eq. (23) is transcendental and must be solved numerically.

Shown in Figure 3 is the maximum midgap voltage shift versus applied field in various limits. The parameters used are consistent with those cited in the literature [8,9]. As seen, when both electron traps and electron injection are neglected, the maximum midgap voltage shift monotonically increases toward a maximum for both the negative and positive applied fields, and the shifts are greater than for all other cases. When electron traps are added, the positive field voltage shift peaks and then decreases at high field. This is due to a lowering of the net charge caused by electron trapping in neutral electron traps. For all values of the field, positive and negative, this result, as might be expected, is lower than the results for no electron trapping.

In the third case we examined, electron trapping by neutral traps has been ignored and electron injection has been included. With no electron trapping by neutral traps, the midgap voltage shift shows no tendency, at the fields examined, to peak and decrease. In order for the midgap voltage shift to peak, a separate electron trap distribution must be present. Neutralization of trapped holes by coulombic capture of electrons by filled hole traps is not sufficient to cause a decrease in the midgap shift at high fields.

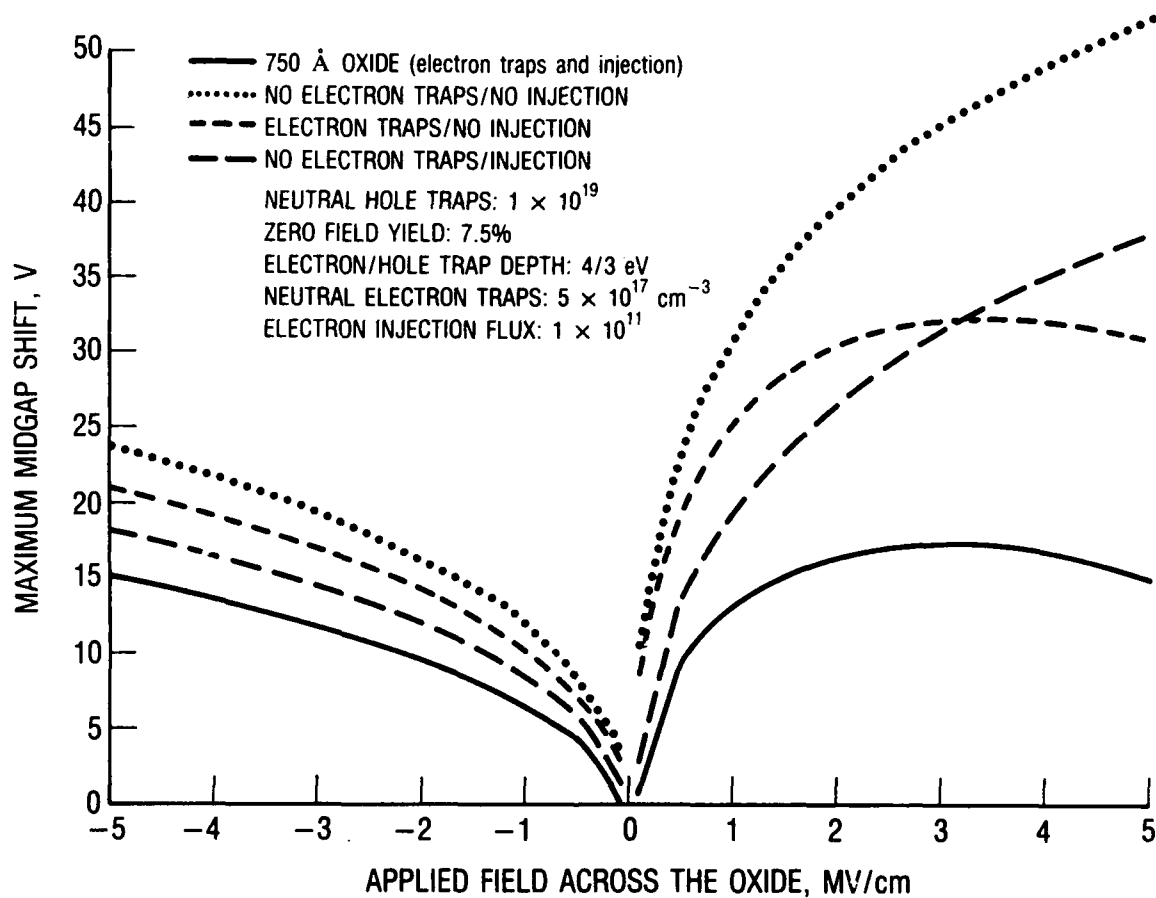


Fig. 3. Theoretical Results for the Maximum Midgap Shift versus Applied Field for a 750 Å Oxide in Various Limits of the Theory.

For comparison we also calculated the maximum midgap shift with both electron injection and electron trapping present, solid curve. When both of these phenomena are included, the voltage shifts are lower than the results in which electron injection is neglected.

III. EXPERIMENTAL COMPARISON

Test capacitors used in this study consisted of thermal oxides of 150, 250, 500, and 750 Å thicknesses grown on p-type silicon, with aluminum gates. The test capacitors were irradiated under bias at room temperature using an ARACOR 10 keV x-ray source. The radiation response of the MOS capacitors was monitored *in situ* using high frequency (1 MHz) capacitance-voltage measurements. The dose rate in all cases was 100 kRad(SiO₂)/min. The threshold voltage shift due to trapped oxide charge was determined as the midgap shift of the post-irradiation C-V measurements.

The midgap voltage shift versus dose data were fitted to an exponential and the initial slope and maximum voltage shift determined for each oxide thickness and various applied voltages. A typical initial slope data set is shown in Figure 4. The data are represented by crosses, and the average uncertainty is represented by open triangles. Shown for comparison are the minimum and maximum uncertainties, which appear as additional crosses on the appropriate data points. The magnitude of the initial slope is plotted versus applied field across the oxide. The applied field was calculated by determining the voltage across the oxide, accounting for the flatband voltage, and dividing by the oxide thickness.

The dashed line is the result of the theory for the parameters listed in the key. These parameters are consistent with values cited in the literature for these types of oxides [8,9]. The electron flux of $1 \times 10^{11} \text{ cm}^{-2}$ is equivalent to $\sim 16 \text{ nA/cm}^2$ and is consistent with previously published values [21]. Electron injection has been invoked at the gate electrode only. As discussed earlier in reference to Figure 1, electron injection has only a limited effect on the initial slope compared to the presence of neutral electron traps.

The steep increase in the initial slope with field is due to the field dependence of the recombination escape probability, which is roughly proportional to the field [1]. This steep increase occurs for both positive and negative fields. At high fields, typical above about 1 MV/cm, the escape probability saturates at unity. Above these fields the decrease in the initial slope is due to the decrease in the hole capture cross section with field [1]. The field dependence of the initial slope at high fields is proportional to one over the square root of the applied field.

The magnitudes of the initial slopes versus applied field for the various thicknesses studied are compiled and shown in Figure 5. The uncertainties are shown for each data set as discussed above. The uncertainty in each data point is less than 20%. In Table 1 we show the parameters used for each oxide thickness to generate the theoretical results, dashed line. Because the initial slope represents the response of the samples at early times (low dose), the pre-irradiation column gives the appropriate hole trap concentration for the initial slopes.

As shown in Figure 5, the positive field theoretical results closely represent the data, whereas the negative field results, while qualitatively representing the data, are by no means as good. We cannot explain this difference, although changing interface conditions with processing could account for the discrepancy.

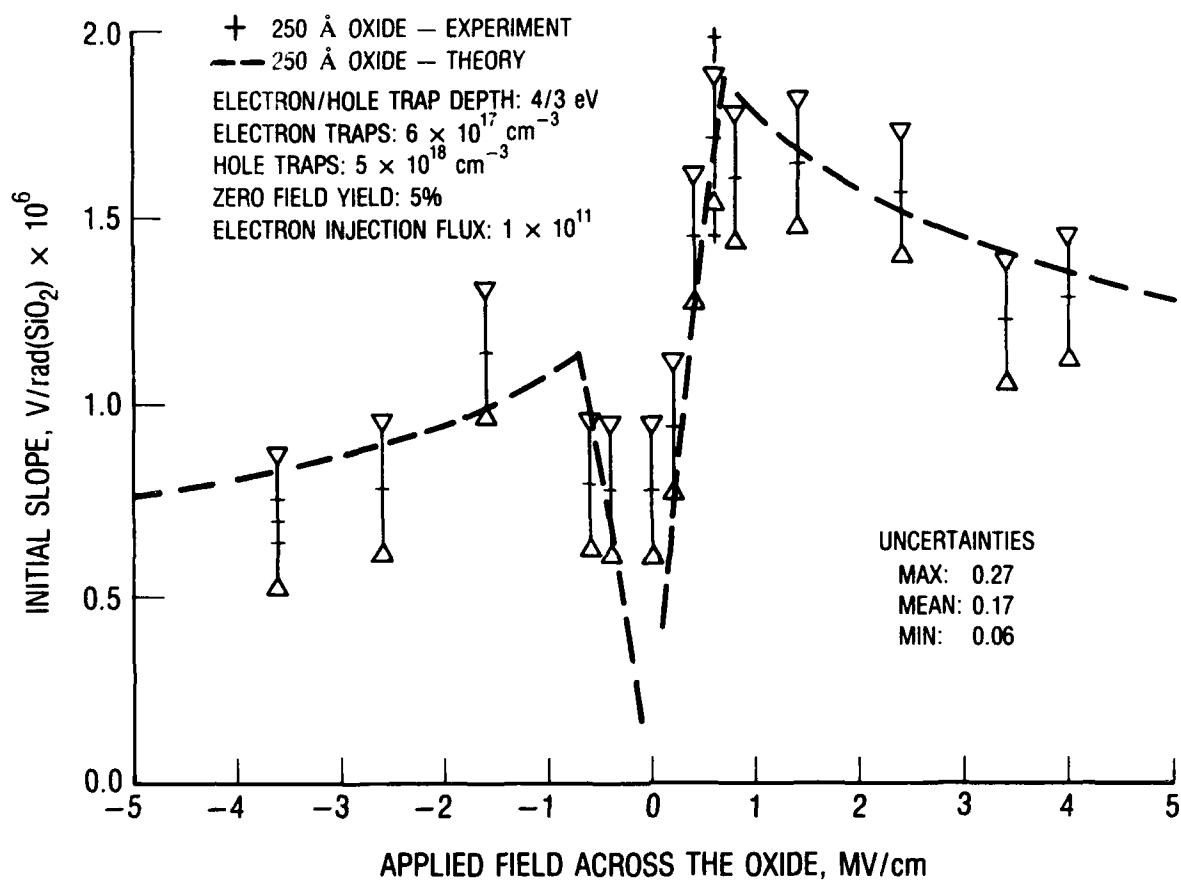


Fig. 4. Typical Data for the Magnitude of the Initial Slope versus Applied Field. The dashed lines are the results of the theory for the parameters cited.

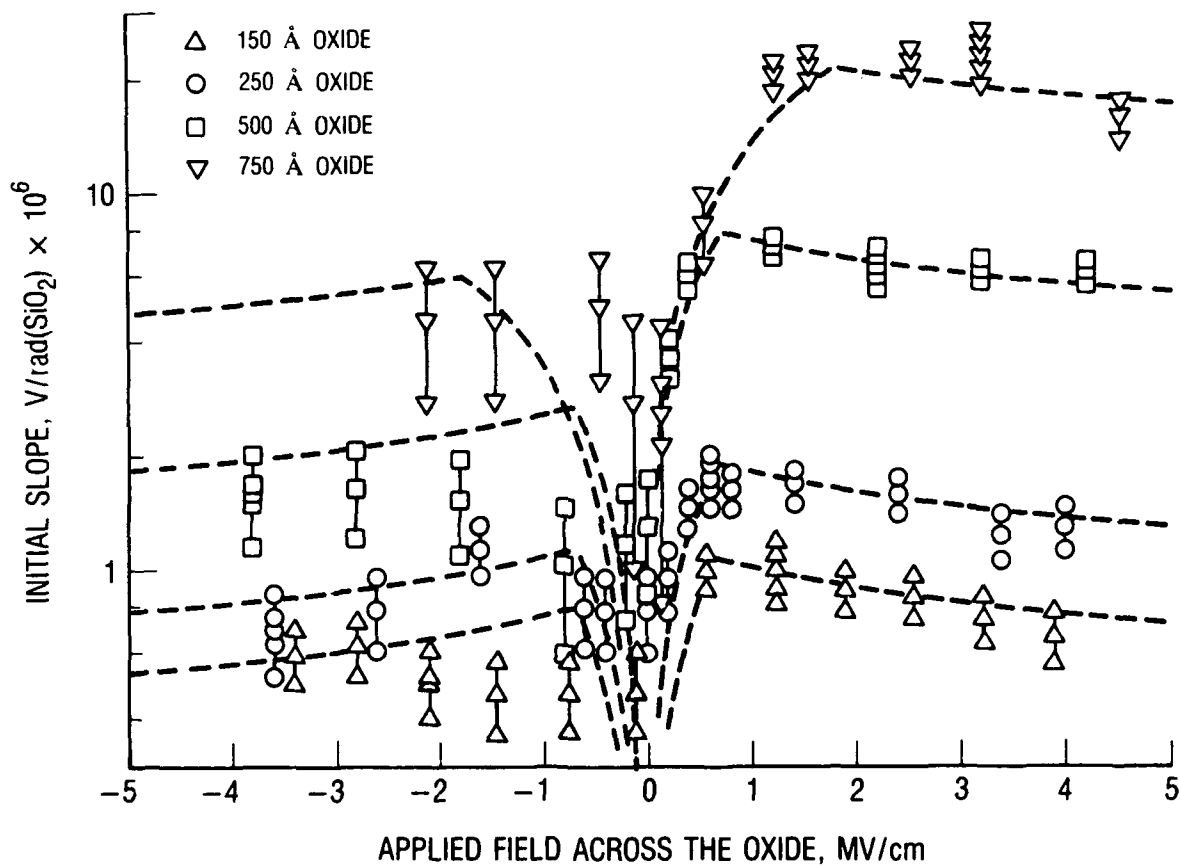


Fig 5. Composite of the Initial Slope versus Applied Field Data for the Oxides Studied. The dashed lines are the results of the theory using parameters listed in Table 1.

Table 1. Parameters Used to Generate Theoretical Results

Oxide Å	Hole Traps (Pre), cm ⁻³	Hole Traps (Post), cm ⁻³	Yield	Electron Traps (Pre/Post)	Electron Injection nA/cm ²
150	1.9 x 10 ¹⁹	6.0 x 10 ¹⁹	5%	6 x 10 ¹⁷	16
250	5.0 x 10 ¹⁸	1.5 x 10 ¹⁹	5%	6 x 10 ¹⁷	16
500	2.2 x 10 ¹⁸	9.0 x 10 ¹⁸	5%	6 x 10 ¹⁷	16
750	2.0 x 10 ¹⁸	7.5 x 10 ¹⁸	2%	6 x 10 ¹⁷	16

The thicker oxides have a larger initial slope than thinner oxides for both positive and negative applied fields. This is expected due to the cubic thickness dependence of the dominant term in Eqs. (14a) and (14b). As the thickness decreases, the initial slope decreases as the cube of the thickness for the larger thicknesses, for which tunneling is less important. As the oxides get thinner, the initial slope dependence on the thickness departs from the simple cubic behavior as tunneling becomes important. Also, as the oxides get thinner, the difference between the positive and negative initial slopes is less pronounced. For thin enough oxides the negative field results can exceed the positive field results. This is because the first moment of the negative field charge distribution can lie closer to the interface than the positive field charge distribution if the tunneling thickness for hole tunneling is large compared to the oxide thickness. The extent of the difference in the initial slopes between the negative and positive field results depends on the details of the distributions.

Figure 6 shows the maximum midgap shift versus field across the oxide for the four oxide thicknesses given. The uncertainty in these data is less than 10%. The same trends are present in these data as for the initial slopes. In each case the positive field maximum midgap shift exceeds the negative field result, because the first moment of the charge distribution is larger for the positive field case. The positive high field results all show a tendency to peak and decrease at the higher fields. As discussed earlier, this is due to the presence of neutral electron traps. The dashed lines are application of Eq. (19a) for the maximum midgap shift using parameters cited in the literature for the escape probability, capture cross sections, trap depths, and injection levels. Table 1 is a compilation of the parameters used to generate the theoretical results. Because the saturated midgap shift represents the response of the samples at long times (high total dose), the post-irradiation trap concentrations apply for these results.

Again, we see that the theory represents the data remarkably well for positive applied fields and only qualitatively for negative applied fields. An important point to note is that the data show a peak in the maximum midgap shift with field and that the theory reflects this behavior. This suggests that there is some worst-case positive field at which to test MOS devices that results in a maximum saturated midgap voltage shift.

As seen in Table 1, as the oxides get thinner the number of hole traps increases. If hole traps are associated with defects in the oxide, the increased strain in the thinner oxides could account for this increase. Also shown in Table 1 is an increase in the number of hole traps with radiation. In all cases there is a three- to four-fold increase in the number of hole traps necessary to represent the

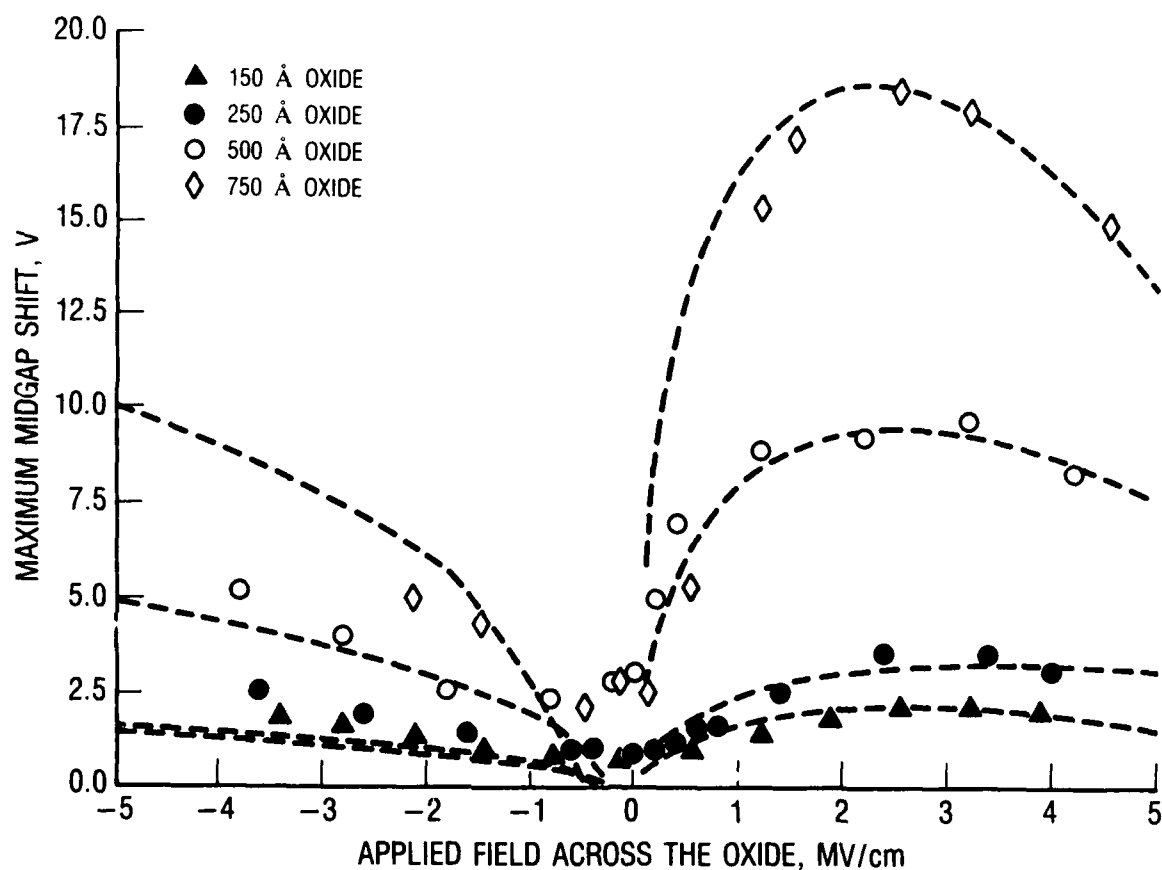


Fig. 6. Composite of the Maximum Midgap Voltage Shift Data for the Oxides Studied. The dashed lines are the results of the theory using parameters listed in Table 1.

post-irradiation data compared to the pre-irradiation data, whereas the electron trap concentration and gate electron injection flux remain constant. The only other difference noted between the behavior of the thin and thick oxides is that the zero field yield for the 750 Å oxide is 2% compared to 5% for the others. We believe this is due to more pre-irradiation fixed charges in the 750 Å oxide than in the other oxides. This is reflected in the fact that the pre-irradiation flatband voltage for the 750 Å oxide was about -3.5 volts, whereas all the other samples had flatband voltages of roughly -1 volt.

IV. SUMMARY

We have extended the theory for the initial slope of the midgap voltage shift and the maximum midgap voltage shift as functions of the applied field in a low dose rate environment to apply to both negative and positive applied fields. The analysis has also been extended to include neutral electron traps, electron injection, and tunneling at low doses. These results show that trapping of electrons by neutral dipole-induced traps is necessary to explain the peak in the positive field saturated midgap shift and that electron injection is necessary to account for the difference in the positive and negative field results as shown by data taken on oxides of varying thicknesses.

REFERENCES

1. R. J. Krantz, L. W. Aukerman, and T. C. Zietlow, "Applied Field and Total Dose Dependence of Trapped Charge Buildup in MOS Devices," *IEEE Trans. Nucl. Sci.* NS-34, No. 6, 1196-1201 (Dec. 1987).
2. H. E. Boesch, F. B. McLean, J. M. Benedetto, J. M. McGarrity, and W. E. Bailey, "Saturation of Threshold Voltage Shifts in MOSFETs at High Total Dose," *IEEE Trans. Nucl. Sci.* NS-33 (Dec. 1986).
3. T. R. Oldham, A. J. Lelis, and F. B. McLean, "Spatial Dependence of Trapped Holes Determined from Tunneling Analysis and Measured Annealing," *IEEE Trans. Nucl. Sci.* NS-33 (Dec. 1986).
4. H. E. Boesch, Jr., and F. B. McLean, "Hole Transport and Trapping in Field Oxides," *IEEE Trans. Nucl. Sci.* NS-32, No. 6, 3940-3945 (Dec. 1985).
5. J. M. Benedetto, H. E. Boesch, Jr., F. B. McLean, and J. P. Mize, "Hole Removal in Thin-Gate MOSFETs by Tunneling," *IEEE Trans. Nucl. Sci.* NS-32, No. 6, 3916-3920 (Dec. 1985).
6. N. S. Saks, M. G. Ancona, and V. A. Modolo, "Radiation Effects in MOS Capacitors with Very Thin Oxides at 80 K," *IEEE Trans. Nucl. Sci.* NS-31, No. 6, 1249-1255 (Dec. 1984).
7. C. M. Dozier and D. B. Brown, "Photon Energy Dependence of Radiation Effects in MOS Structures," *IEEE Trans. Nucl. Sci.* NS-27, No. 6, 1694-1699 (Dec. 1980).
8. A. R. Stivers and C. T. Sah, "A Study of Oxide Traps and Interface States of the Silicon-Silicon Dioxide Interface," *J. Appl. Phys.* 51(12), 6292-6304 (Dec. 1980).
9. D. J. DiMaria, in *The Physics of SiO₂ and Its Interfaces*, edited by S. T. Pantelides (Pergamon, New York 1978), pp. 160-178.
10. J. M. Aitken and D. R. Young, "Electron Trapping in Electron-beam Irradiated SiO₂," *J. Appl. Phys.* 49(6), 3386-3391 (June 1978).
11. J. M. Aitken and D. R. Young, "Avalanche Injection of Holes into SiO₂," *IEEE Trans. Nucl. Sci.* NS-24, No. 6, 2128-2134 (Dec. 1977).
12. J. M. Aitken and D. R. Young, "Electron Trapping by Radiation-induced Charge in MOS Devices," *J. Appl. Phys.* 47, 1196-1198 (Mar. 1976).
13. F. B. McLean, H. E. Boesch, Jr., and J. M. McGarrity, "Hole Transport and Recovery Characteristics of SiO₂ Gate Insulators," *IEEE Trans. Nucl. Sci.* NS-23, No. 6, 1506-1512 (Dec. 1976).
14. J. R. Srour, S. Othmer, O. L. Curtis, Jr., and K. Y. Chiu, "Radiation-induced Charge Transport and Charge Buildup in SiO₂ Films at Low Temperatures," *IEEE Trans. Nucl. Sci.* NS-23, No. 6, 1513-1519 (Dec. 1976).
15. H. E. Boesch, Jr., and J. M. McGarrity, "Charge Yield and Dose Effects in MOS Capacitors at 80 K," *IEEE Trans. Nucl. Sci.* NS-23, 1520-1525 (Dec. 1976).
16. J. M. Aitken, D. J. DiMaria, and D. R. Young, "Electron Injection Studies of Radiation Induced Positive Charge in MOS Devices," *IEEE Trans. Nucl. Sci.* NS-23, No. 6, 1526-1533 (Dec. 1976).

17. H. E. Boesch, Jr., F. B. McLean, J. M. McGarrity, and G. A. Ausman, "Hole Transport and Charge Relaxation in Irradiated SiO₂ MOS Capacitors," *IEEE Trans. Nucl. Sci. NS-22*, No. 6, 2163-2167 (Dec. 1975).
18. E. H. Snow, A. S. Grove, B. E. Deal, and C. T. Sah, "Ion Transport Phenomena in Insulating Films," *J. Appl. Phys.* 36(5), 1664-1673 (May 1965).
19. M. Lenzlinger and E. H. Snow, "Fowler-Nordheim Tunneling into Thermally Grown SiO₂," *J. Appl. Phys.* 40(1), 278-283 (Jan. 1969).
20. R. J. Krantz and W. L. Bloss, "Strong Inversion Model of Threshold Voltage in Modulation Doped Field Effect Transistors: The Role of Unintentional Acceptors," Submitted to *IEEE Trans. Electron Devices*.
21. M. R. Chin and T. P. Ma, "Photocurrent Generation in Thermal SiO₂ Under X-Ray Irradiation," *J. Appl. Phys.* 53(5), 3673-3679 (May 1982).

LABORATORY OPERATIONS

The Aerospace Corporation functions as an "architect-engineer" for national security projects, specializing in advanced military space systems. Providing research support, the corporation's Laboratory Operations conducts experimental and theoretical investigations that focus on the application of scientific and technical advances to such systems. Vital to the success of these investigations is the technical staff's wide-ranging expertise and its ability to stay current with new developments. This expertise is enhanced by a research program aimed at dealing with the many problems associated with rapidly evolving space systems. Contributing their capabilities to the research effort are these individual laboratories:

Aerophysics Laboratory: Launch vehicle and reentry fluid mechanics, heat transfer and flight dynamics; chemical and electric propulsion, propellant chemistry, chemical dynamics, environmental chemistry, trace detection; spacecraft structural mechanics, contamination, thermal and structural control; high temperature thermomechanics, gas kinetics and radiation; cw and pulsed chemical and excimer laser development including chemical kinetics, spectroscopy, optical resonators, beam control, atmospheric propagation, laser effects and countermeasures.

Chemistry and Physics Laboratory: Atmospheric chemical reactions, atmospheric optics, light scattering, state-specific chemical reactions and radiative signatures of missile plumes, sensor out-of-field-of-view rejection, applied laser spectroscopy, laser chemistry, laser optoelectronics, solar cell physics, battery electrochemistry, space vacuum and radiation effects on materials, lubrication and surface phenomena, thermionic emission, photo-sensitive materials and detectors, atomic frequency standards, and environmental chemistry.

Computer Science Laboratory: Program verification, program translation, performance-sensitive system design, distributed architectures for spaceborne computers, fault-tolerant computer systems, artificial intelligence, micro-electronics applications, communication protocols, and computer security.

Electronics Research Laboratory: Microelectronics, solid-state device physics, compound semiconductors, radiation hardening; electro-optics, quantum electronics, solid-state lasers, optical propagation and communications; microwave semiconductor devices, microwave/millimeter wave measurements, diagnostics and radiometry, microwave/millimeter wave thermionic devices; atomic time and frequency standards; antennas, rf systems, electromagnetic propagation phenomena, space communication systems.

Materials Sciences Laboratory: Development of new materials: metals, alloys, ceramics, polymers and their composites, and new forms of carbon; non-destructive evaluation, component failure analysis and reliability; fracture mechanics and stress corrosion; analysis and evaluation of materials at cryogenic and elevated temperatures as well as in space and enemy-induced environments.

Space Sciences Laboratory: Magnetospheric, auroral and cosmic ray physics, wave-particle interactions, magnetospheric plasma waves; atmospheric and ionospheric physics, density and composition of the upper atmosphere, remote sensing using atmospheric radiation; solar physics, infrared astronomy, infrared signature analysis; effects of solar activity, magnetic storms and nuclear explosions on the earth's atmosphere, ionosphere and magnetosphere; effects of electromagnetic and particulate radiations on space systems; space instrumentation.